Journal of
Marine Science and Engineering

MDPI

Article

Investigation of the Hydrodynamic Characteristics of Two Manta Rays Tandem Gliding

Yunlong Ma [1,2], Qiaogao Huang [1,2,*], Guang Pan [1,2] and Pengcheng Gao [1,2]

[1] School of Marine Science and Technology, Northwestern Polytechnical University, Xi'an 710072, China
[2] Key Laboratory of Unmanned Underwater Vehicle, Northwestern Polytechnical University, Xi'an 710072, China
* Correspondence: huangqiaogao@nwpu.edu.cn

Abstract: Collective motion is a unique biological habit of manta rays. As the most basic unit, the hydrodynamic mechanism of tandem gliding deserves further study. In this paper, a numerical simulation method was used to explore the influence of the front-to-back distance and the angle of attack on the overall and individual hydrodynamic performance of a pair of manta rays gliding. Specifically, a numerical simulation of the hydrodynamic parameters and the distribution of pressure and velocity fields was carried out when the pair of manta rays were arranged at a distance of 0.25–1 times the body length and the angle of attack was −8° to 8°. The simulation results show that, when a pair of manta rays glide at close range, compared to a single manta ray gliding, the resistance of the leader is greatly reduced, and the lift changes little, while the resistance of the follower is greatly increased, and the lift is significantly reduced. For the average resistance of the system, in the specific scenario of a close range and a small negative degree angle of attack, the two manta rays' tandem gliding system can significantly reduce the resistance and play a role in reducing resistance and saving energy. The research content of this paper provides a theoretical basis for understanding the biological habits of manta rays and designing an underwater bionic robot group system.

Keywords: manta rays; fish schooling; tandem gliding; hydrodynamic characteristics

Citation: Ma, Y.; Huang, Q.; Pan, G.; Gao, P. Investigation of the Hydrodynamic Characteristics of Two Manta Rays Tandem Gliding. *J. Mar. Sci. Eng.* **2022**, *10*, 1186. https://doi.org/10.3390/jmse10091186

Academic Editor: Abdellatif Ouahsine, Alberto Ribotti, Peng Du, Haibao Hu, Xiaopeng Chen

Received: 8 July 2022
Accepted: 20 August 2022
Published: 25 August 2022

1. Introduction

Long-term natural evolution has endowed fish with extraordinary movement and survivability: long-distance cruise with low energy consumption, high-efficiency propulsion with large thrust, powerful explosive force and maneuverability, sensitive perception and positioning capabilities, excellent self-protection and precise attack capabilities. Manta rays are ray-like creatures with flat bodies, large aspect ratios, and cruising speeds of 0.25–0.47 m/s [1]. The Median and/or Paired Fin (MPF) mode is the steady-state cruising mode of manta rays [2], and the efficiency can be as high as 89%, which is higher than that of aquatic organisms such as eels and trevallies [3,4]. It has extraordinary advantages in mobility and concealment. Manta rays have obvious shape features, efficient propulsion performance, and energy-saving group swimming, which give them great bionic value.

Collective motion is a common phenomenon in fish biology [5], which is also present in manta ray species. Studies have shown that, for fish, swimming in groups is usually more efficient than swimming alone. In nature, more than 50% of fishes exhibit synchronized and coordinated group swimming at some point [6]. When migrating, many fish swim in groups in the same direction and maintain a near-constant separation from their neighbors [7]. In addition to the sociological advantages of avoiding natural enemies [8,9] and improving the success rate of predation [10–12], group swimming is also considered to be effective in reducing energy consumption [13–17].

In view of the high efficiency and energy-saving characteristics of fish group swimming, researchers have conducted a lot of research hoping to reveal the inherent mechanism

of fluid mechanics. At present, the common research methods are as follows: 1. Fish colony observation method; 2. Computational fluid dynamics simulation method; 3. Experimental research method using bionic robotic fish.

The fish colony observation method used in earlier periods, due to the limitation of equipment and technology, mainly used the observation of the swimming characteristics of fish combined with the method of hydrodynamic theoretical analysis. Breder was the first to study the energy-saving mechanism of fish swimming. He believed that the complete wake vortex structure scale was an important factor affecting the distribution interval of individuals [18]. With the continuous development of observation technology, high-speed cameras and digital particle image velocimetry technology are used more and more by researchers to extract and observe the performance information, morphological structure, and eddy current characteristics of fish schools. Then, the energy consumption data can be obtained through theoretical calculation or DPIV experiment, so as to reveal the energy-saving mechanism of fish swimming. Marras et al., tested the collective motion of liza aurata at different flow rates and found that individuals in the best position in the flock reduced their tail-wagging frequency by up to 28.5% compared to swimming alone. It was also found by DPIV that the swing of an anterior individual helps its neighboring fishes to swim forward [19].

With the continuous development of computer technology and fluid simulation technology, the method of computational fluid dynamics is more and more widely used in the study of the mechanism of fish school energy saving. Unlike the observation method, which can only obtain some qualitative conclusions, the CFD simulation method can quantitatively measure the force of each individual in the fish group more accurately, making the analysis results more reliable and intuitive. Pan et al. [20], Shao et al. [21], and Xiao et al. [22,23] used the immersion boundary method to numerically simulate the passive motion of the flexible plate behind the D-shaped cylinder. The former can obtain thrust from the wake vortex of the former, which greatly improves the propulsion efficiency; Chao et al. [24,25] used a commercial CFD software package to numerically simulate the double-body system of a D-shaped cylinder and a NACA0012 flexible plate. It was found that the thrust of the downstream airfoil was improved due to the presence of the cylinder. Based on the theory of potential flow and viscosity, Fish et al., estimated the propulsion efficiency of manta rays and found that most of the thrust is generated by the distal end of the fin during its movement [26]. Zhang Dong et al., used the immersion boundary method to simulate the process of a manta ray flapping and advancing and explored the influence of motion parameters, such as flapping amplitude and frequency, on its propulsion effect [27].

On the basis of the first two methods, some researchers have begun to design experimental devices in recent years hoping to study the energy-saving mechanism of fish swimming through experimental methods. Dewey [28] and Boschitsch [29] experimentally studied the propulsion characteristics of two parallel and series flapping airfoils in a uniform incoming flow, respectively. The experimental system investigates the effects of wing-flap phase difference and separation distance. The study found that, for the tandem structure, the thrust and efficiency of the front wing were consistent with the single wing shape when the separation distance was large, while the dynamic characteristics of the rear wing were related to the separation distance and phase difference due to the influence of the wake of the front wing. For the parallel configuration, the propulsion characteristics of the two airfoils are the same: when flapping in-phase, efficiency increases and thrust decreases (relative to a single airfoil); when flapping in anti-phase, thrust increases while efficiency remains largely unchanged.

From the current research status, it can be seen that most of the work focuses on two-dimensional airfoils or flexible sheets, rather than on real three-dimensional creatures. Moreover, the research mainly focuses on the group travel over the two-dimensional plane and does not consider the effect of a real three-dimensional situation on the results. For the two-body tandem system, less research has been done on underwater targets, and more research has been focused on the water surface or in the air. Zhang Dong et al., used

the CFD method to study the hydrodynamics of rotary underwater vehicles in series and gave the law of mutual influence between the front and rear individuals [30,31]. Yuan, Zhi-Ming et al., simplified the swimmer's model, used the CFD method to simulate the swimming process in an actual competition, and gave the law of influence of resistance on the back of the athlete with the distance [32]. Using the same method, they simplified the duck model to explain the hydrodynamic reasons why ducklings swim with their mother ducks in nature [33]. Blocken et al., used a combination of CFD and experiments to study the process of two cyclists following movement back and forth and gave the advantages of the two-body system and the wind resistance law of each single body [34]. None of the previous studies involved the simulation of manta rays group gliding, and this issue has not been systematically studied, so it is innovative and scientific to a certain extent. Research on the energy-saving mechanism of collective motion can, on the one hand, give us a deeper understanding of animal habits, and on the other hand, can provide inspiration and help for the design and control of underwater robots, especially underwater bionic robots, so as to improve operational efficiency and to develop and utilize marine resources more efficiently. Therefore, this paper focuses on a real, three-dimensional manta ray pair's tandem gliding system, explores the gliding hydrodynamic performance of manta rays at different distances, reveals the hydrodynamic mechanism of biological long-distance schooling fish migration, and provides a theoretical basis for the group design of underwater bionic robots.

The second chapter describes the goals and problems of the simulation and verifies the calculation method and grid independence. The third chapter records the simulation results, analyzes the hydrodynamic characteristics of the manta ray pair's gliding system., compares it with the single manta ray, and gives a formation scheme that can reduce resistance. The fourth chapter summarizes the full text and lists all the important conclusions.

2. Problem Definition and Methodology

2.1. Biological Model and Reference Dimensions

Through the real observation of the biological shape of the cow-nosed ray and three-dimensional software modeling, the final numerical simulation target model was obtained as shown in Figure 1. The dimensions of each model were defined as follows: body length (BL) = 1800 mm, spanwise length (SL) = 2900 mm, and maximum thickness length (TL) = 350 mm. This paper takes BL as the reference length and BL^2 as the reference area.

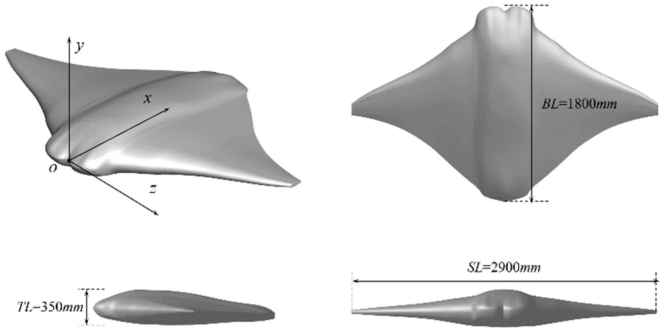

Figure 1. The 3D model of a manta ray.

2.2. Simulation Method Validation

In order to ensure the correctness of the numerical simulation results, the calculation method was first verified. At present, domestic and foreign scholars have not carried out numerical simulation work on manta ray gliding. In addition, the model has an irregular shape, a high proportion of curved surfaces, and is difficult to process, which can only be obtained by additive manufacturing. Machining the model and performing wind-tunnel or water-tunnel experiments on it would have disadvantages, such as a high cost and long time, which do not meet the requirements of previous mechanistic research. Therefore, the method of CFD simulation was used to study this problem. Observing

the shape characteristics of the manta ray, it can be seen that its topology is similar to the three-dimensional hydrofoil. The scholar Zarruk [35] experimentally measured the hydrodynamic parameters of a graphical model 3D hydrofoil with different materials, Reynolds number (*Re*), and angle of attack (α). The root chord length of the model was 0.12 m, the wing chord length was 0.06 m, and the spread length was 0.3 m. The average chord length of 0.09 m was taken as the reference length. For this model, the grid was drawn as shown in Figure 2. The numerical simulation method and turbulence model of SST *k*-*ω* in this paper was used to calculate the variation, with the angle of attack law for the three-dimensional hydrofoil lift coefficient and resistance coefficient when the Reynolds number is 1×10^6. ν is the kinematic viscosity coefficient of water, which is 1.003×10^{-6}. The simulation results were compared with the experimental values, and the results are shown in Figure 3. It can be seen that the simulation results were in good agreement with the experimental data, indicating that the calculation method used in this paper has great reliability.

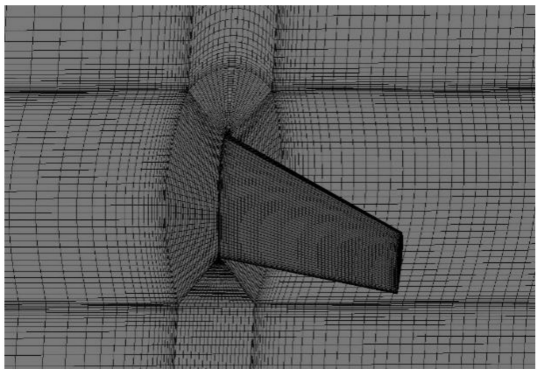

Figure 2. Grid of hydrofoil model for method validation.

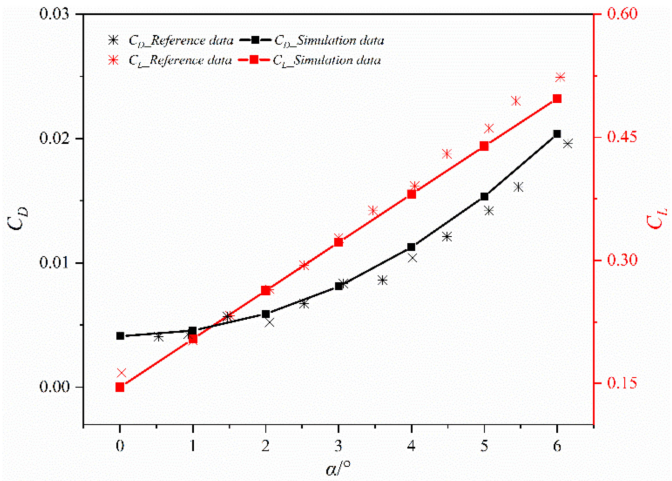

Figure 3. Method validation and comparison results.

2.3. Grid Independence Validation

The numerical simulation results are closely related to the number of cells. In order to ensure the correctness of the manta ray gliding simulation, it was necessary to carry out grid-independent verification. Draw the manta ray structure grid as shown in Figure 4. The typical y^+ value of the first grid point near the manta ray surface was set as 1, and the *Re* was 9×10^5. The overall grid distribution density was changed and the lift and resistance values of the manta ray model was recorded for different numbers of cells, as shown in Figure 5. It can be concluded from Figure 5 that, when the number of cells is small, the lift and resistance values under the same working conditions change drastically with the increase in the number of cells. When the number of cells reaches 4.5×10^6, the lift

and resistance values no longer change with the grid number. On the premise of ensuring the reliability of the simulation results, in order to improve the calculation efficiency and save simulation time, the grids of all subsequent working conditions were drawn using the node distribution law with the number of cells being 4.5×10^6. The number of cells of the manta ray pair system increases to 6.1×10^6 due to the addition of one individual and will further grow as the distance between the two manta rays increases.

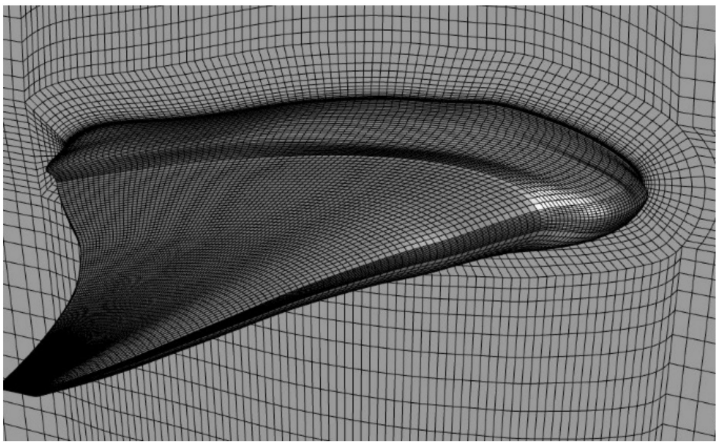

Figure 4. Structure grid of manta ray.

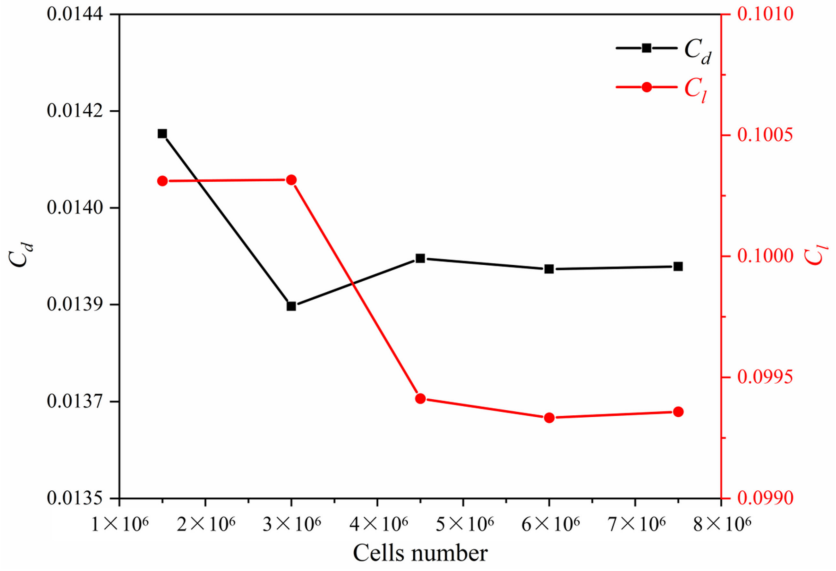

Figure 5. Simulation results under different numbers of cells.

In order to explore the hydrodynamic characteristics of the manta ray pair's tandem gliding system, the structure grid was drawn as shown in Figure 6. The two manta rays were distributed forward and backward along the x-axis, and the distance between the tail of the leader and the head of the follower was defined as Δs, which is measured as a multiple of the BL. Since the structure of the manta ray model was symmetrical, in order to reduce the number of cells and improve the calculation efficiency, half of the grid domain was drawn. The boundary condition on the left side was set as the symmetry plane, so the numerical simulation of the whole can be completed. In addition, the front side was set as the velocity inlet, the rear side was set as the pressure outlet, the surface of the manta ray model was set as a non-slip wall, and the other surfaces were set as free-slip walls. The overall computational domain was a cuboid. The height was set as 20 TL; the width was set as 2 SL; the leader's head was 4 BL from the velocity inlet; the follower's tail was 7 BL

from the pressure outlet. The computational domain size and boundary condition settings are shown in Figure 6.

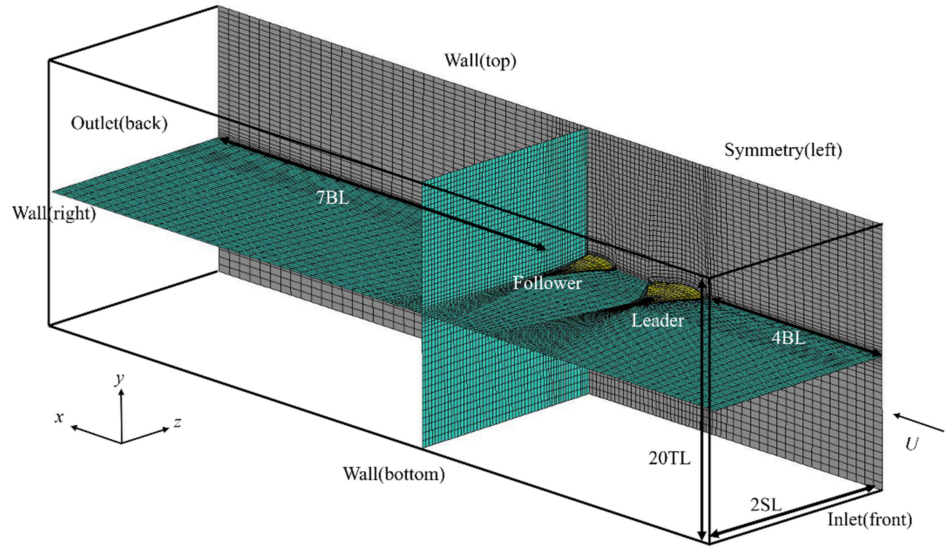

Figure 6. Computational domain size and boundary condition settings.

2.4. Simulation Domain and Boundary Condition Settings

After completing the grid-drawing work, we simulated the conditions by numerical simulation method. The finite volume method was used to discretize the Navier-Stokes equation, the second-order upwind style was used to discretize the momentum, the derivative was calculated based on the least-squares method, and the SIMPLEC algorithm was used to calculate the pressure in the continuous equation. As for the selection of the turbulence model, Lyu Da et al., used the SST k-ω model to accurately simulate the hydrodynamic parameters of the flying wing underwater glider [36]. The manta ray model in this study has certain similarities with the flying wing underwater glider. The related content regarding method verification in Section 2.2 also shows that the SST k-ω turbulence model can accurately simulate the underwater airfoil problem. In summary, we used the SST k-ω turbulence model for simulation calculations, and the convergence residual was set to 1×10^{-5}.

3. Result and Discussion

In this section, we compare and analyze the hydrodynamic performance differences between a single manta ray and a pair of manta rays when gliding at different angles of attack and consider the influence of distance on the system when two manta rays tandem glide. The resistance of the manta ray was defined as D and the lift as L. The above parameters were non-dimensionalized as:

$$C_D = \frac{D}{0.5\rho U^2 (BL)^2}, C_L = \frac{L}{0.5\rho U^2 (BL)^2} \quad (1)$$

where ρ is the density of the water, which was set to 1000 kg/m^3; U is the incoming velocity, which was set to 0.5 m/s; BL is the reference length. The Reynolds number at this time was calculated to be 9×10^5.

The average resistance and coefficient of the system was defined as:

$$D_{ave-system} = (D_{leader} + D_{follower})/2, \; C_{D_{ave-system}} = \frac{D_{ave-system}}{0.5\rho U^2 (BL)^2} \quad (2)$$

3.1. Numerical Simulation Results of a Single Manta Ray

In this part, we first study the hydrodynamic performance of a single manta ray gliding. Figure 7 shows the variation of the resistance coefficient and lift coefficient with the angle of attack when the manta ray is gliding. It can be seen from Figure 7 that in the range of −8 to 8° angle of attack, the lift received by the manta ray increases linearly with the change of the angle of attack, and the resistance shows a quadratic function with the angle of attack. It can be clearly seen from Figure 8 that the manta ray has a relatively flat lower surface and a raised upper surface in terms of biological structure. Therefore, when the angle of attack is 0°, the water velocity near the upper surface of the manta ray is fast, and the water velocity near the lower surface is slow. Therefore, the pressure difference in the vertical direction of the upper and lower surfaces causes the manta ray to experience a small lift at this time. When the angle of attack is −2°, the water velocity distribution near the upper and lower surfaces is relatively close, so the vertical pressure difference is small. Therefore, the lift force is approximately equal to 0, and the resistance on the manta ray reaches the minimum value at this time.

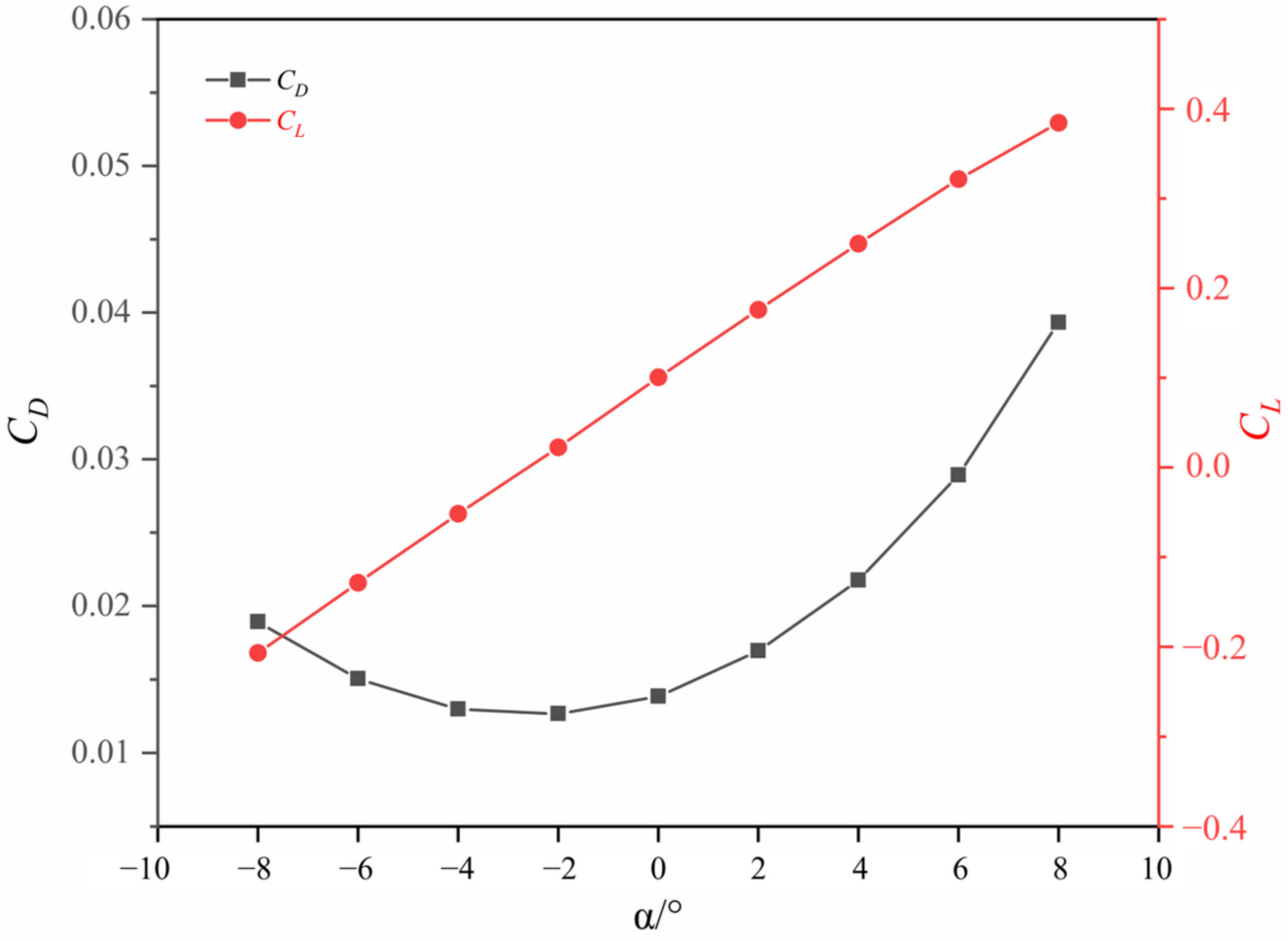

Figure 7. Variation of a single manta ray gliding: resistance coefficient and lift coefficient with angle of attack.

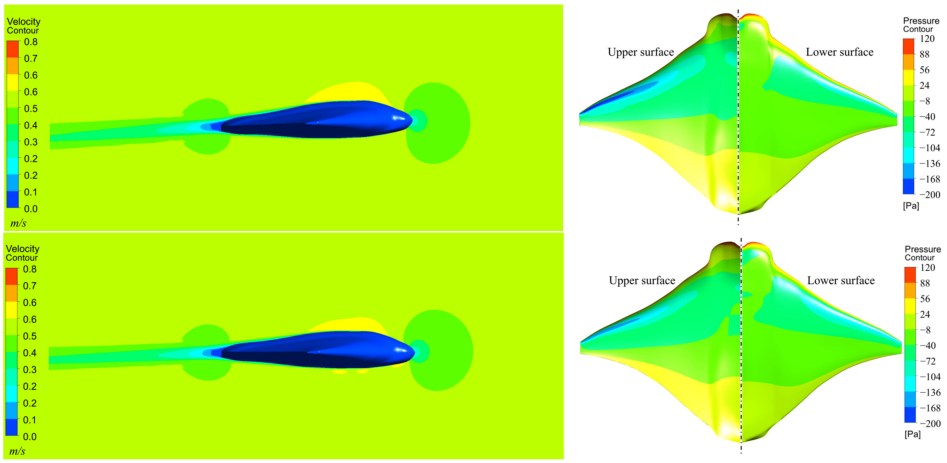

Figure 8. Longitudinal symmetry plane velocity distribution and manta ray surface pressure distribution during single gliding at $\alpha = 0°$ (**up**) and $\alpha = -2°$ (**down**).

3.2. Numerical Simulation Results of Two Manta Rays Tandem

This part studies the differences in the hydrodynamic performance of two manta rays gliding. As shown in Figure 6, the leader manta ray and the follower manta ray are arranged horizontally along the *x*-axis, and the angle of attack changes synchronously from −8 to 8°. The hydrodynamic performance at the distances Δs = 0.25 BL, 0.5 BL, 0.75 BL, 1 BL were simulated, respectively, and the results are shown in Figure 9.

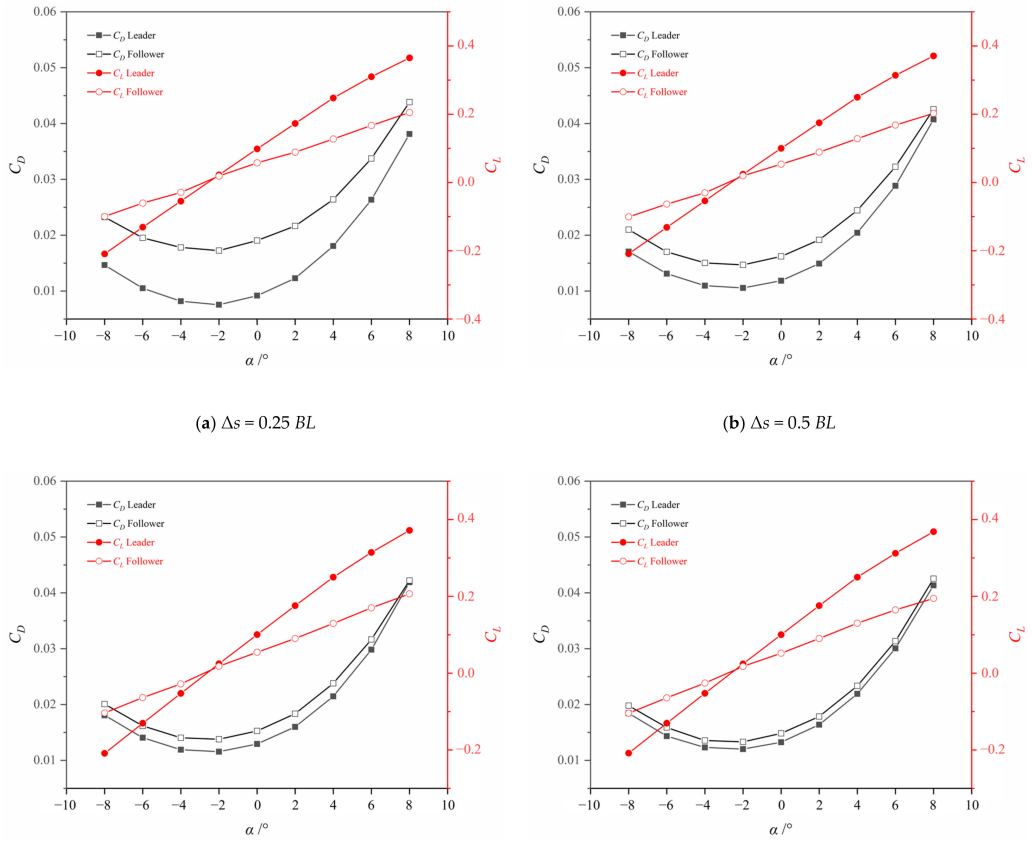

(**a**) Δs = 0.25 *BL* (**b**) Δs = 0.5 *BL*

(**c**) Δs = 0.75 *BL* (**d**) Δs = 1 *BL*

Figure 9. The variation of the resistance coefficient and lift coefficient with the angle of attack of two manta rays at different distances.

It can be seen from Figure 9 that, when the pair of manta rays are arranged horizontally along the *x*-axis, the hydrodynamic performance trend of each individual remains unchanged. The lift received by the manta ray increases linearly with the change of the angle of attack, and the resistance shows a quadratic function with the angle of attack. However, for the leader, compared with the single manta ray gliding, the resistance is greatly reduced, and the lift force is slightly increased, while for the follower, the resistance force is greatly increased, and the lift force is greatly reduced. This phenomenon—that the resistance of the leader decreases and the resistance of the follower increases—is close to the conclusion of Zhang et al. [30,31]. For targets on the water surface, such as swimmers or ducks, their followers can greatly reduce resistance with the help of the team [32,33], which is contrary to our conclusion. In addition, some studies have found that, when two cyclists ride in tandem, the resistance of each individual, whether the leader or the follower, is less than that of a single person. This conclusion is also different from our research results [34]. The main reason some results obtained from the above studies are different from our conclusions is that the research targets are located in different media and environments.

It is worth noting that, as the distance between the leader and the follower increases, the resistance of each individual quickly converges to the resistance data of a single manta ray, while the difference in lift decreases very slowly. Taking an angle of attack of 4° as an example, when the distance is 0.25 BL, the resistance of the follower is about 1.47 times that of the leader, and the lift is 51.5% that of the leader. When the distance increases to 1 BL, the resistance of the follower decreases to 1.06 times that of the leader, while the lift is 52.1% that of the leader, showing an increase of only 0.6%. In the process of increasing the distance, for the resistance value, the leader increases and the follower decreases to the single manta ray situation, respectively. For the lift value, the leader is not affected from the beginning, and it is always the same as the single manta ray situation; while the follower is strongly affected by the leader at close range and returns to the single manta ray level slowly, as shown in Figure 10. To summarize, for the manta ray tandem system, the resistance value of the manta ray is more sensitive to a change in the distance, and the lift value changes very slowly with the increase in the distance.

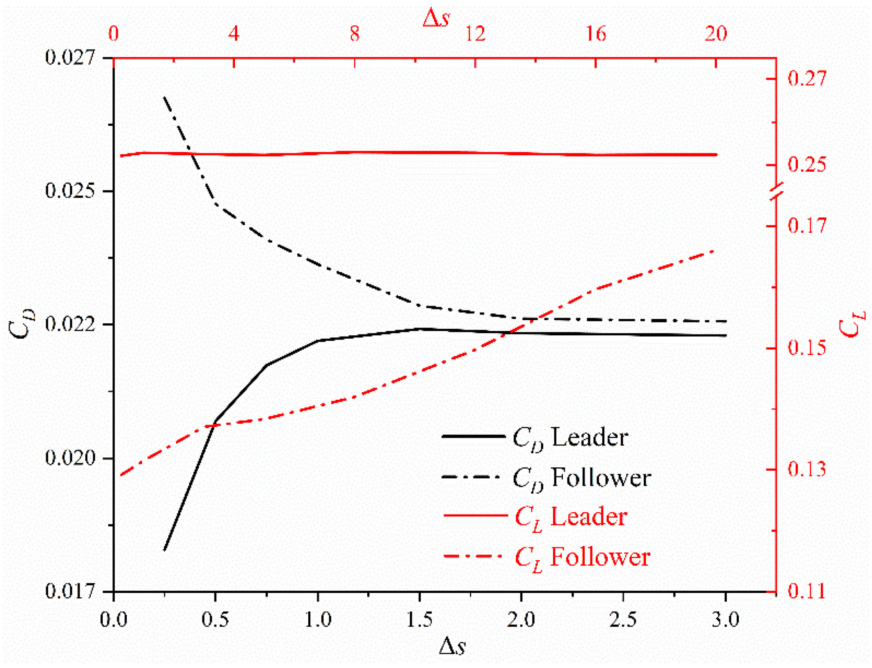

Figure 10. The variation of the gliding resistance coefficient and lift coefficient of two manta rays with distance at $\alpha = 4°$.

3.3. Analysis of Resistance Reduction Effect and Flow Field Mechanism

This part explores the hydrodynamic performance of the tandem gliding system under the influence of the two manta rays. Figure 11 shows the average resistance of the system $\overline{D}_{system}$ relative to the resistance of a single manta ray when gliding under different distances and angles of attack. It can be seen from Figure 11 that, for most working conditions, the average resistance of the system is higher than that of the single case. After 2° angle of attack, the relative value of average system resistance gradually increases with the increase in attack angle. For example, when the angle of attack is 8° and Δs is 1 BL, the average resistance of the system is about 6.6% higher than that of the single case. It shows that, in most cases, the average resistance of the pair of manta rays' tandem system is higher than the single manta ray's resistance, and the energy consumption of the system increases. Interestingly, however, we found that when the angle of attack is −6° to −2°, the average resistance of the system is lower than the single resistance at some certain distance cases, which can play a role in reducing resistance and saving energy. For example, when the angle of attack is −2° and Δs is 0.25 BL, the average resistance of the system is about 2.3% lower than that of the single manta case.

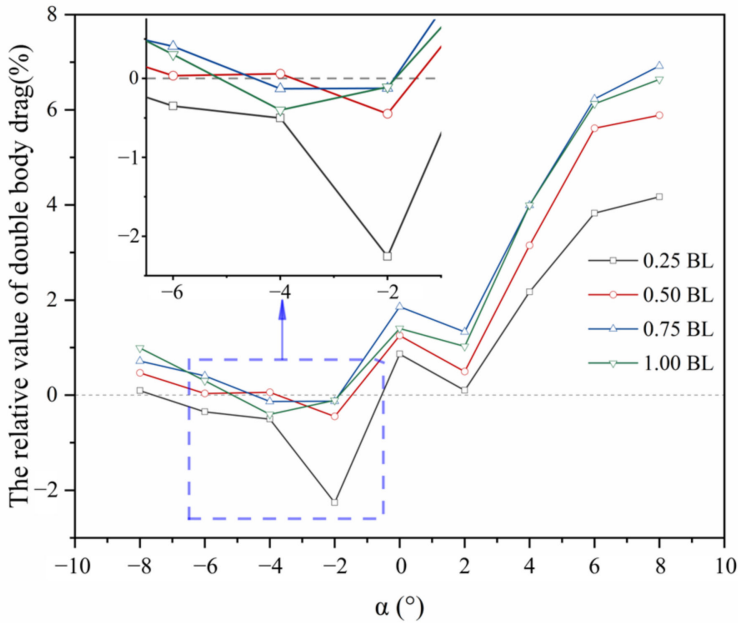

Figure 11. Relative value of the two manta rays gliding system average resistance coefficient.

In order to explore the fluid mechanism of the average resistance of the system, we give the pressure and velocity distribution of $\alpha = -2°$, $\Delta s = 0.25$ BL and $\alpha = 8°$, $\Delta s = 1$ BL, respectively, as shown in Figures 12 and 13. Figure 12 shows the surface pressure distribution of the tandem manta rays at $\alpha = -2°$, $\Delta s = 0.25$ BL, and the velocity distribution of some section planes are also given in the figure. Comparing Figures 8 and 12a, it can be seen that a continuous low-speed zone is formed between the tail of the leader and the head of the follower. Due to the presence of this area, the pressure on the leader's tail and the follower's head increases. Under the premise of little change in the rest, the front-to-back pressure difference of the leader decreases, resulting in decreased resistance. The front-to-back pressure difference of the follower increases, resulting in increased resistance. As for the overall system, the low-speed area at the tail of the leader has not closed and disappeared, and it is affected by the follower and continues to develop backward. Therefore, a coherent high-pressure area is formed between the leader and the follower, as shown in Figures 12 and 13, which makes the average resistance of the system decrease slightly.

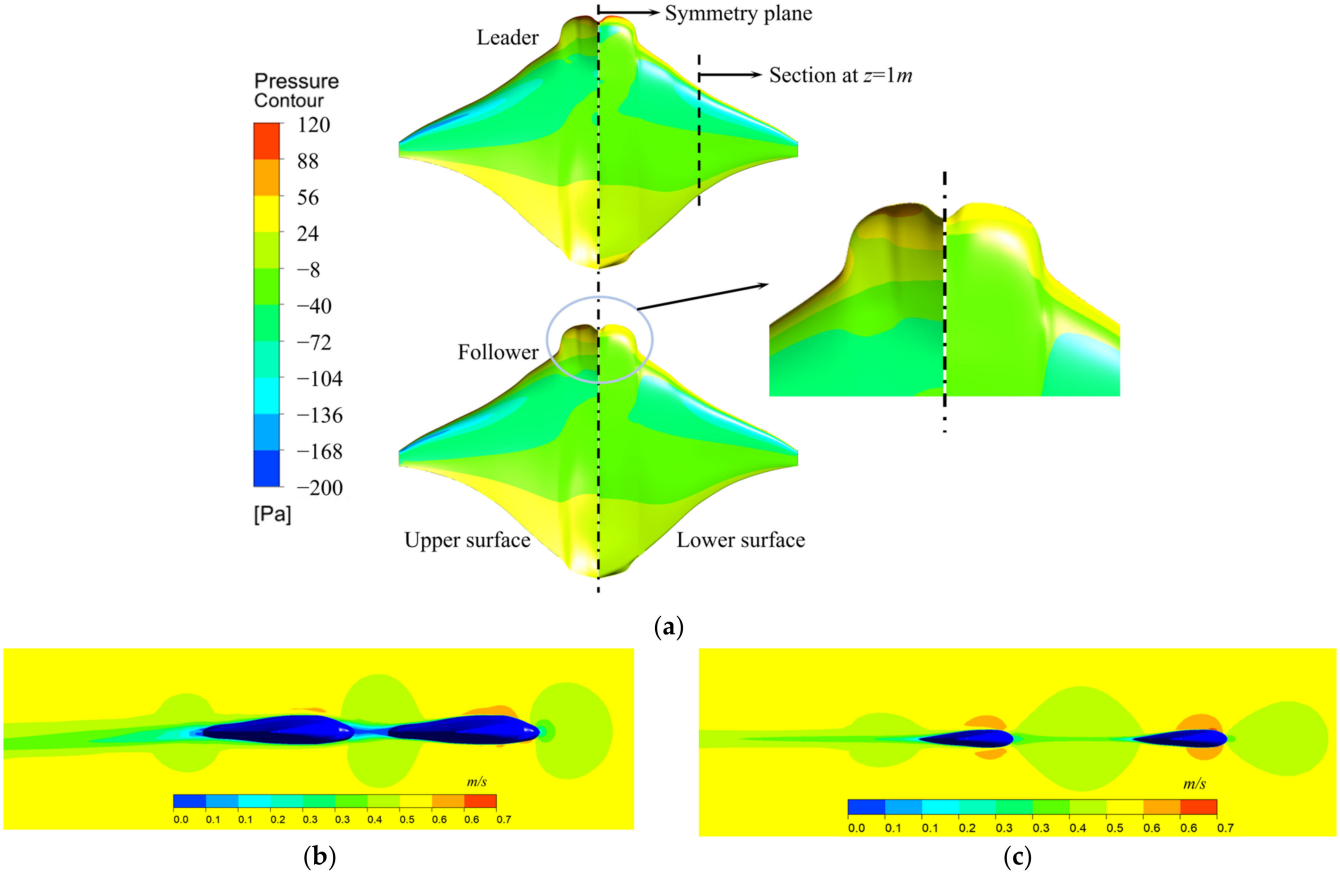

Figure 12. Surface pressure distribution and typical cross-sectional velocity distribution of two manta rays tandem system at $\alpha = -2^\circ$, $\Delta s = 0.25$ BL. (**a**): Surface pressure distribution. (**b**): Velocity distribution of symmetry plane. (**c**): Velocity distribution of section at $z = 1$ m.

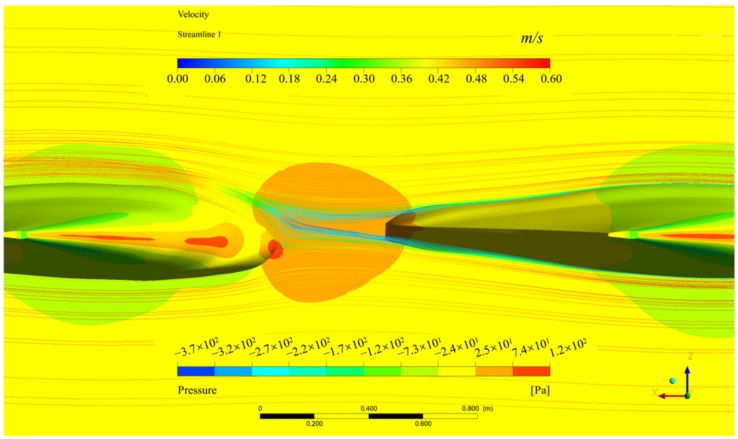

Figure 13. Surface pressure distribution and streamline diagram of the symmetry plane of two manta rays tandem system at $\alpha = -2^\circ$, $\Delta s = 0.25$ BL.

Figure 14a shows the surface pressure distribution of the tandem manta ray at $\alpha = 8^\circ$, $\Delta s = 1$ BL, and Figure 14b,c shows the velocity distribution of some section planes. Compared with the single manta ray gliding at 8°, the tail flow field of the leader and the lower flow field of the follower have obvious mutual influence. For the leader, superimposing the large distance factor, its surface pressure distribution is almost unaffected, so its lift and resistance are not much different from those of the single gliding; for the follower, the low-pressure area on the upper surface is significantly reduced, and the high-pressure area on the lower surface expands. The pressure difference between the front and rear leads

to an increase in the resistance, and the pressure difference between the upper and lower sides decreases, so that the lift force is greatly reduced.

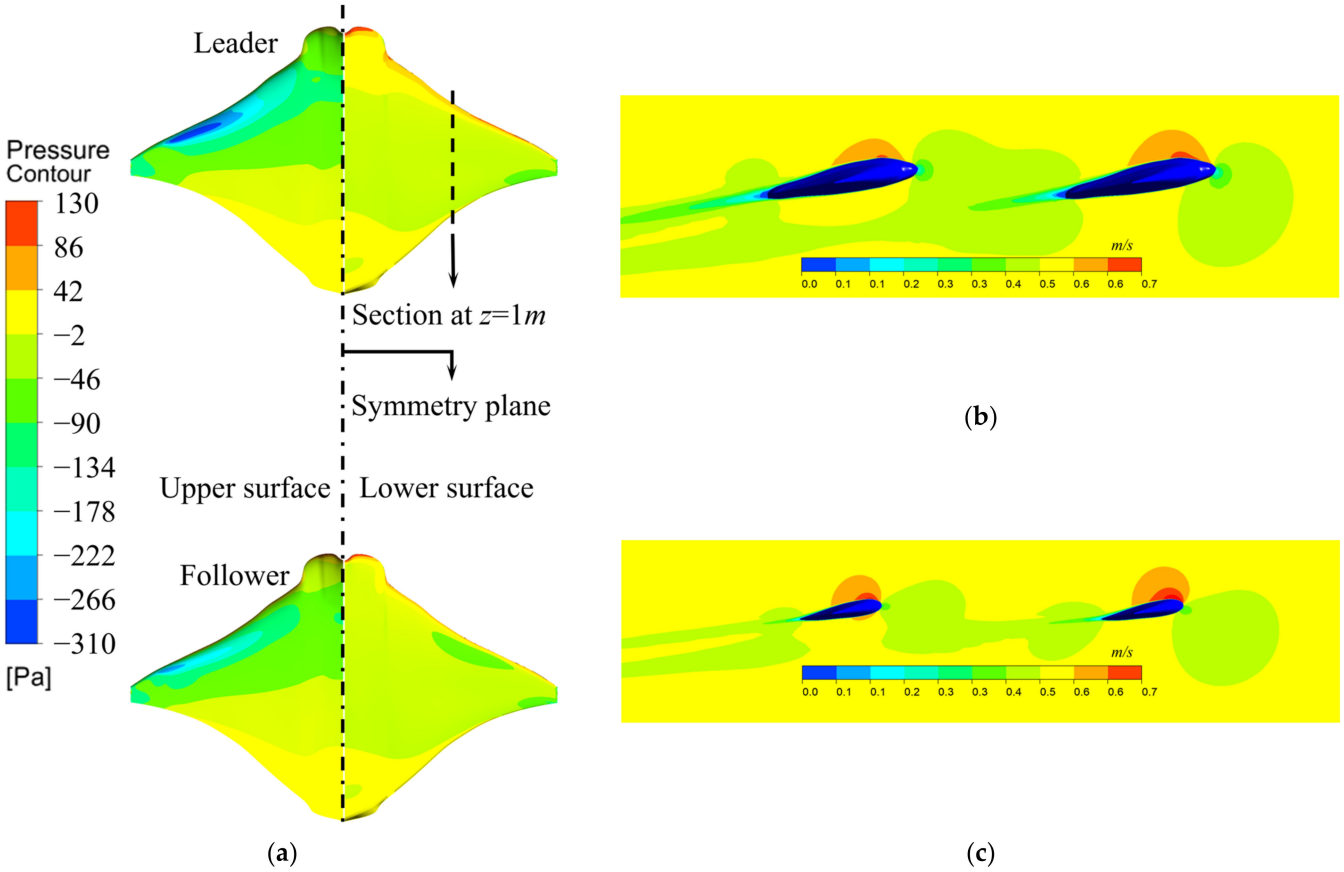

Figure 14. Surface pressure distribution and typical cross-sectional velocity distribution of two manta rays tandem system at $\alpha = 8°$, $\Delta s = 1$ BL. (**a**): Surface pressure distribution. (**b**): Velocity distribution of symmetry plane. (**c**): Velocity distribution of section at $z = 1$ m.

4. Conclusions

In order to explore the hydrodynamic mechanism behind the group swimming phenomenon during the biological migration of manta rays in nature, we used a numerical simulation method to systematically analyze the basic group swimming component of a two-body tandem. The changes in hydrodynamic parameters and surrounding pressure field and velocity field when two manta rays glide at different distances and angles of attack were mainly discussed. The variation law of each individual and group in the two manta rays system under different working conditions was obtained, which provides a strong theoretical support for understanding the collective motion habits of manta rays and the group formation design of underwater bionic vehicles. The main simulation conclusions are as follows:

1. When a single manta ray glides, the lift coefficient is a linear function of the angle of attack, and the resistance coefficient is a quadratic function of the angle of attack. This law does not change when two manta rays are gliding in series. Whether it is the leader or the follower, the lift coefficient and resistance coefficient change with the same angle of attack, and the difference lies in the magnitude of the value.
2. In the two manta rays tandem system, compared with the single-body gliding, the resistance of the leader is greatly reduced, and the lift of the leader is almost unchanged, while for the follower, the resistance is greatly increased, and the lift is greatly reduced.

3. With the increase in the distance between the front and rear of the two manta rays, the resistance of the leader increases rapidly, and the resistance of the follower decreases rapidly, and the two tend to be the same; in terms of lift, the leader maintains the lift regardless of the distance. The lift is stable, not much different from the single-body gliding situation. The lift experienced by the follower is greatly reduced when the distance is small, and the growth recovers slowly with the increase in the distance.
4. For the average resistance of the system, in the specific scenario of a close-range, small negative degree angle of attack, the double manta rays series system can effectively reduce the resistance and play a role in reducing resistance and saving energy. For example, when the distance between the front and rear of the double manta rays is $\alpha = -2^\circ$, $\Delta s = 0.25$ BL, and the two attitudes maintain a -2° angle of attack, the average resistance of the system is reduced by about 2.3% compared with the single resistance. This is of great significance for understanding biological habits and designing underwater bionic vehicle group formations.

According to the above research results of a manta ray pair's tandem gliding, perhaps in the future, when unmanned underwater vehicles travel in groups, due to the increase in the resistance of the leader, we need to pay more attention to the energy consumption of the leader. Change the group formation in time, or let the leader carry more energy. It should be pointed out that the hydrodynamic characteristics of the two manta rays gliding are only the most basic and smallest unit in the study of manta ray group swimming. In our future series of research, we will further consider the problem of manta rays group swimming with more individuals, more complex movement modes, and multiple formations so as to reveal the hydrodynamic characteristics behind the group swimming of this species.

Author Contributions: Writing-original draft, Y.M.; study design, Y.M. and Q.H.; data collection, Y.M. and P.G.; data analysis, Y.M. and P.G.; review & editing, Q.H. and G.P.; supervision, G.P. All authors have read and agreed to the published version of the manuscript.

Funding: This work was supported by the National Natural Science Foundation of China (Grant No. 51879220 and 52001260), the National Key Research and Development Program of China (Grant No. 2020YFB1313201), Fundamental Research Funds for the Central Universities (Grant No. 3102019HHZY030019 and 3102020HHZY030018), and Innovation Foundation for Doctor Dissertation of Northwestern Polytechnical University (CX2022025).

Institutional Review Board Statement: Not applicable.

Informed Consent Statement: Not applicable.

Data Availability Statement: Not applicable.

Conflicts of Interest: The authors declare no conflict of interest.

References

1. Rosenberger, L.J. Pectoral fin locomotion in batoid fishes: Undulation versus oscillation. *J. Exp. Biol.* **2001**, *204*, 379–394. [CrossRef] [PubMed]
2. Graham, R.T.; Witt, M.; Castetllanos, D.W.; Remolina, F.; Maxwell, S.; Godley, B.; Hawkes, L. Satellite tracking of manta rays highlights challenges to their conservation. *PLoS ONE* **2012**, *7*, e36834. [CrossRef] [PubMed]
3. Borazjani, I.; Fotis, S. Numerical investigation of the hydrodynamics of carangiform swimming in the transitional and inertial flow regimes. *J. Exp. Biol.* **2008**, *211*, 1541–1558. [CrossRef] [PubMed]
4. Breder, J.; Charles, M. The locomotion of fishes. *Zoologica* **1926**, *4*, 159–291. [CrossRef]
5. Weihs, D. Hydromechanics of fish schooling. *Nature* **1973**, *241*, 290–291. [CrossRef]
6. Shaw, E. Schooling fishes: The school, a truly egalitarian form of organization in which all members of the group are alike in influence, offers substantial benefits to its participants. *Am. Sci.* **1978**, *66*, 166–175.
7. Pitcher, T.J. Functions of shoaling behaviour in teleosts. In *The Behaviour of Teleost Fishes*; Springer: Boston, MA, USA, 1986; pp. 294–337.
8. Godin, J.J.; Joanne, M. Predator avoidance and school size in a cyprinodontid fish, the banded killifish (*Fundulus diaphanus* Lesueur). *Behav. Ecol. Sociobiol.* **1985**, *16*, 105–110. [CrossRef]
9. Magurran, A.E.; Anthony, H. Information transfer across fish shoals under predator threat. *Ethology* **1988**, *78*, 153–158. [CrossRef]
10. Pitcher, T.J.; Magurran, A.E.; Winfield, I.J. Fish in larger shoals find food faster. *Behav. Ecol. Sociobiol.* **1982**, *10*, 149–151. [CrossRef]

11. Wolf, N.G. Schooling tendency and foraging benefit in the ocean surgeonfish. *Behav. Ecol. Sociobiol.* **1987**, *21*, 59–63. [CrossRef]
12. Ranta, E.; Kai, L. Assortative schooling in three-spined sticklebacks? *Ann. Zool. Fenn.* **1990**, *27*, 67–75.
13. Fish, F.E. Energetics of swimming and flying in formation. *Comments Theor. Biol.* **1999**, *5*, 283–304.
14. Herskin, J.; Steffensen, J.F. Energy savings in sea bass swimming in a school: Measurements of tail beat frequency and oxygen consumption at different swimming speeds. *J. Fish Biol.* **1998**, *53*, 366–376. [CrossRef]
15. Johansen, J.L.; Vaknin, R.; Stetffensen, J.F.; Domenici, P. Kinematics and energetic benefits of schooling in the labriform fish, striped surfperch *Embiotoca lateralis*. *Mar. Ecol. Prog. Ser.* **2010**, *420*, 221–229. [CrossRef]
16. Killen, S.S.; Maunrras, S.; Stetffensen, J.F.; McKenzie, D.J. Aerobic capacity influences the spatial position of individuals within fish schools. *Proc. R. Soc. B Biol. Sci.* **2012**, *279*, 357–364. [CrossRef] [PubMed]
17. Ross, R.M.; Thomas, W.H.B.; Karin, E.L. Group-size-mediated metabolic rate reduction in American shad. *Trans. Am. Fish. Soc.* **1992**, *121*, 385–390. [CrossRef]
18. Breder, C.M. Vortices and fish schools. *Zool. Sci. Contrib. N. Y. Zool. Soc.* **1965**, *50*, 97–114. [CrossRef]
19. Marras, S.; Killen, S.S.; Lindström, J.; McKenzie, D.J.; Steffensen, J.F.; Domenici, P. Fish swimming in schools save energy regardless of their spatial position. *Behav. Ecol. Soc.* **2014**, *69*, 219–226. [CrossRef]
20. Pan, D.Y.; Hua, L.; Shao, X.M. Studies on the oscillation behavior of a flexible plate in the wake of a D-cylinder. *J. Hydrodyn.* **2010**, *22*, 132–137. [CrossRef]
21. Shao, X.; Pan, D.; Deng, J.; Yu, Z. Hydrodynamic performance of a fishlike undulating foil in the wake of a cylinder. *Phys. Fluids* **2010**, *22*, 111903.
22. Shao, X.; Pan, D.; Deming, J.; Yu, Z. Computational study on near wake interaction between undulation body and a D-section cylinder. *Ocean. Eng.* **2011**, *38*, 673–683.
23. Xiao, Q.; Wendi, L.; Hu, J. Parametric study on a cylinder drag reduction using downstream undulating foil. *Eur. J. Mech. B/Fluids* **2012**, *36*, 48–62. [CrossRef]
24. Chao, L.M.; Zhang, D.; Cao, Y.-H.; Pan, G. Numerical studies on the interaction between two parallel D-cylinder and oscillated foil. *Mod. Phys. Lett. B* **2018**, *32*, 1850034. [CrossRef]
25. Chao, L.M.; Pan, G.; Zhang, D.; Yan, G.X. On the thrust generation and wake structures of two travelling-wavy foils. *Ocean. Engin.* **2019**, *183*, 167–174. [CrossRef]
26. Fish, F.E.; Schreiber, C.M.; Moored, K.W.; Liu, G.; Dong, H.; Bart-Smith, H. Hydrodynamic performance of aquatic flapping: Efficiency of underwater flight in the manta. *Aerospace* **2016**, *3*, 20. [CrossRef]
27. Zhang, D.; Huang, Q.-G.; Pan, G.; Yang, L.-M.; Huang, W.-X. Vortex dynamics and hydrodynamic performance enhancement mechanism in batoid fish oscillatory swimming. *J. Fluid Mech.* **2022**, *930*, A28. [CrossRef]
28. Dewey, P.A.; Quinn, D.B.; Boschitsch, B.M.; Smits, J. Propulsive performance of unsteady tandem hydrofoils in a side-by-side configuration. *Phys. Fluids* **2014**, *26*, 041903. [CrossRef]
29. Boschitsch, B.M.; Peter, A.; Alexander, J.S. Propulsive performance of unsteady tandem hydrofoils in an in-line configuration. *Phys. Fluids* **2014**, *26*, 051901. [CrossRef]
30. Zhang, D.; Liming, C.; Guang, P. Analysis of hydrodynamic interaction impacts on a two-AUV system. *Ships Offshore Struct.* **2019**, *14*, 23–34. [CrossRef]
31. Zhang, D.; Pan, G.; Shi, Y.; Wang, P.; Chao, L. Investigation of the resistance characteristics of a multi-AUV system. *Appl. Ocean. Res.* **2019**, *89*, 59–70. [CrossRef]
32. Yuan, Z.-M.; Pan, G.; Shi, Y.; Wang, P.; Chao, L. Stseady hydrodynamic interaction between human swimmers. *J. R. Soc. Interface* **2019**, *16*, 59–70. [CrossRef]
33. Yuan, Z.-M.; Li, M.; Ji, C.-Y.; Li, L.; Jia, L.; Cetcik, L. Wave-riding and wave-passing by ducklings in formation swimming. *J. Fluid Mech.* **2021**, *928*, 820. [CrossRef]
34. Blocken, B.; Defraeye, T.; Koninckx, E.; Carmeliet, J.; Hespel, P. CFD simulations of the aerodynamic drag of two drafting cyclists. *Comput. Fluids* **2013**, *71*, 435–445. [CrossRef]
35. Zarruk, G.A.; Brandner, P.A.; Pearce, B.W.; Phillips, A.W. Experimental study of the steady fluid-structure interaction of flexible hydrofoils. *J. Fluids Struct.* **2014**, *51*, 326–343. [CrossRef]
36. Lyu, D.; Song, B.; Pan, G.; Yuan, Z.; Li, J. Winglet effect on hydrodynamic performance and trajectory of a blended-wing-body underwater glider. *Ocean Eng.* **2019**, *188*, 106303. [CrossRef]